

20 with laboratory measurements of sand samples collected at nine pseudo-invariant sand dune sites
21 located in the western/southwestern USA. The nine sand dune sites cover a broad range of surface
22 emissivities in the TIR. Results show that the absolute mean emissivity difference between NAALSED
23 and the laboratory results for the nine validation sites and all five ASTER TIR bands was 0.016 (1.6
24 %). This emissivity difference is equivalent to approximately a 1 K error in the land surface
25 temperature for a material at 300 K in the TIR.

26

27 **1. INTRODUCTION**

28

29 The Advanced Spaceborne Thermal Emission and Reflection Radiometer (ASTER) was
30 launched on the Terra satellite in December 1999 and has five bands in the Thermal Infrared (TIR)
31 with a spatial resolution of 90 m. Remote sensing observations of narrowband surface emissivity in the
32 wavelength range covered by ASTER TIR bands 10-14 centered on 8.3, 8.6, 9.1, 10.6, and 11.3 μm
33 respectively range from ~ 0.65 to close to 1.0 for most natural Earth surfaces. Narrowband emissivities
34 over arid and semi-arid areas in the 8-12 μm range typically have large variation due to the strong
35 quartz absorption feature (Reststrahlen band) in the 8-9.5 μm region, whereas the emissivity of dense
36 vegetation, water and ice cover is greater than 0.95 and constant in the 8-12 μm range. Changes in
37 surface emissivity for most natural surfaces occur primarily due to variations in soil moisture (Mira et
38 al. 2007), vegetation cover and type (French et al. 2008), and surface roughness (Mushkin and
39 Gillespie 2005), of which the influence of soil moisture is the least understood.

40 Land Surface Temperature and Emissivity products (LST&E) are generated by spaceborne
41 sensors such as the Atmospheric Infrared Sounder (AIRS) (Susskind et al. 2003), the Moderate-
42 Resolution Imaging Spectrometer (MODIS) (Wan 2008) and ASTER (Gillespie et al. 1998; Hulley et

43 al. 2008). Although these emissivity products produce the same measure, there are often discrepancies
44 between them due to their varying spatial, spectral and temporal resolutions, and the different
45 algorithms used to retrieve the surface emissivity.

46 LST&E products are key parameters used in land surface dynamics, climate modeling, and
47 surface-atmosphere interactions. In climate modeling, recent sensitivity tests based on the NCAR
48 Community Land Model (Bonan et al. 2002) indicate that an emissivity error of 0.1 (10 %) in barren
49 areas such as Northern Africa and the Arabian Peninsula will result in current climate models having
50 errors of up to 6.6 Wm^{-2} in their upward longwave radiation estimates (Jin and Liang 2006; Zhou et al.
51 2003). This represents a much larger term than the surface radiative forcing due to an increase in
52 greenhouse gases ($\sim 2\text{-}3 \text{ Wm}^{-2}$), making accurate knowledge of the surface emissivity a critical
53 component for climate change studies.

54 In surface-atmosphere interactions, errors in the retrievals of atmospheric temperature and
55 moisture profiles from hyperspectral infrared radiances, such as those from AIRS, are strongly
56 dependent on the accuracy of the surface emissivity (Kornfield and Susskind 1977), particularly over
57 arid and semi-arid regions where the variation in emissivity is large, both spatially and spectrally (Li et
58 al., 2007). Using a baseline-fit (BF) model based on laboratory measurements to fill in spectral gaps in
59 the MOD11 emissivity product, Seemann et al. (2008) found that the MOD07 total precipitable water
60 (TWP) retrieval biases were reduced from 2.1 mm to 0.2 mm when using the BF method as opposed to
61 assuming a constant emissivity of 0.95.

62 While the land surface temperature products from ASTER have been validated by several
63 authors (Coll et al. 2005; Hook et al. 2007; Tonooka and Palluconi 2005), far fewer authors have
64 attempted to validate the surface emissivity product (Schmugge and Ogawa 2006; Schmugge et al.
65 2003). In this study we have validated the North American ASTER Land Surface Database

66 (NAALSED) v2.0 emissivity product over arid/semi-arid regions using nine pseudo-invariant sand
67 dune sites in the western/southwestern USA. The emissivity of samples collected at each of the nine
68 sites was determined in the laboratory using a Nicolet 520 FT-IR spectrometer (Baldrige et al., 2009)
69 and convolved with the appropriate ASTER system response functions. Validation of emissivity data
70 from space ideally requires a site that is homogeneous in emissivity at the scale of the imagery,
71 allowing several image pixels to be validated over the target site. ASTER is able to meet this
72 requirement due to its high spatial resolution of 90 m, making it unique amongst other spaceborne
73 sensors that provide emissivity products at much coarser spatial resolutions. Validating the ASTER
74 emissivity product with ground truth opens up the opportunity for validating other LST&E products
75 from MODIS (5 km) and AIRS (45 km), by down-sampling the ASTER data over large homogeneous
76 areas.

77 The nine sand dune validation sites chosen for this study were: Great Sands National Park,
78 Colorado; White Sands National Monument, New Mexico; Kelso Dunes, California; Algodones
79 Dunes, California; Stovepipe Wells Dunes, California; Coral Pink Sand Dunes, Utah; Little Sahara
80 Dunes, Utah; Killpecker Dunes, Wyoming; and Moses Lake Basalt Dunes, Washington.

81

82 **2. THE NORTH AMERICAN ASTER LAND SURFACE EMISSIVITY DATABASE**

83 **(NAALSED) V2.0**

84

85 Using the results from the Temperature Emissivity Separation Algorithm (TES) (Gillespie et al.
86 1998), a mean seasonal ASTER LST&E database has been produced at 100 m spatial resolution
87 referred to as the North American ASTER Land Surface Emissivity Database (NAALSED) (Hulley
88 and Hook 2009b). The database can be ordered from <http://emissivity.jpl.nasa.gov> and covers the

89 winter months of minimum vegetation cover (Jan-Mar) and summer months of maximum vegetation
90 cover (Jul-Sep). Hulley et al. (2008) provide a detailed description of NAALSED (version 1.0) and
91 initial results for California and Nevada, while Hulley and Hook, (2008) describe a new methodology
92 for ASTER cloud screening in NAALSED. In the two seasonal datasets the emissivity is calculated as
93 the average emissivity of all clear-sky pixels for a given location from all scenes acquired in the season
94 over the entire current period of acquisition of ASTER data (2000-2008). Figure 1 shows the
95 NAALSED summer emissivity product for ASTER band 12 (9.1 μm) covering USA and Mexico and
96 generated by using a total of 70,075 ASTER scenes.

97 The NAALSED v2.0 product consists of eighteen bands: the mean and standard deviation of
98 the surface emissivity (all five TIR ASTER bands), surface temperature, Normalized Difference
99 Vegetation Index (NDVI), a Land-Water Map (LWM), the total yield, and geodetic latitude and
100 longitude. Currently the database is available from 25-49° N, 125-66° W, and processing is currently
101 underway for the rest of North America from 49-84° N, 169-52° W, including Alaska and Canada.

102

103 **3. SAND DUNE FIELD VALIDATION**

104

105 The following sections describe the stability of the sand dune validation sites with regard to
106 spatial uniformity and temporal stability; the methodology for collecting sand samples in the field and
107 measuring the emissivity in the laboratory; and a comparison of NAALSED emissivities with the
108 laboratory results is then discussed. Table 1 provides a summary highlighting the location, formation
109 and basic geology of the nine dune sites used in the study.

110

111 **3.1 Long-term Stability**

112

113 Pseudo-invariant ground sites such as playas, salt flats and claypans have been increasingly
114 recognized as optimal targets for the long-term validation and calibration of visible, shortwave and
115 thermal infrared data (Bannari et al. 2005; Cosnefroy et al. 1996; de Vries et al. 2007; Teillet et al.
116 1998). We have found that large sand dune fields are also useful for the validation of TIR emissivity
117 data (Hulley and Hook 2009a). Sand dunes have consistent and homogeneous mineralogy and
118 physical properties over long time periods, they don't collect water for long periods as playas and pans
119 might, and drying of the surface does not lead to cracks and fissures which could raise the emissivity
120 due to cavity radiation effects (Mushkin and Gillespie 2005). Furthermore, the mineralogy and
121 composition of sand samples collected in the field can be accurately determined in the laboratory using
122 reflectance and X-Ray Diffraction (XRD) measurements.

123 The long-term temporal stability of the dunes is a critical aspect since NAALSED is a multi-
124 year, mean seasonal emissivity product, and does not reflect inter-annual variations in emissivity other
125 than in the standard deviation for a given pixel provided with the product. In general the dune sites
126 should be spatially uniform and any temporal variability due to changes in soil moisture and vegetation
127 cover should be minimal. Ideally the surface should always be dry, since any water on the surface can
128 increase the emissivity by up to 0.16 (16%) in the 8.2 – 9.2 μm range depending on the type of soil
129 (Mira et al. 2007).

130 Seasonal changes in vegetation cover, aeolian processes such as wind erosion, deposition and
131 transport, and daily variations in surface soil moisture from precipitation, dew, and snow-melt are the
132 primary factors that could potentially affect the temporal stability and spatial uniformity of the dune
133 sites. Table 2 shows a summary of the temporal and spatial variations of NDVI and band 11 (8.6 μm)
134 emissivity for pixels extracted from NAALSED at each sampling site for all dune fields. Band 11 was

135 chosen because of low atmospheric absorption effects as compared to band 10, and also the sensitivity
136 of the quartz Reststrahlen band (8-9.5 μm) to soil moisture. The average sampling site consisted of 100
137 ASTER pixels (1 km \times 1 km). Values shown are the total number of observations, mean NDVI from
138 NAALSED, temporal standard deviation in NDVI (δNDVI), temporal standard deviation ($\delta\epsilon_t$) and
139 spatial variation ($\delta\epsilon_s$) in emissivity using all ASTER observations from 2000-2008. Results from
140 Table 2 will be discussed in the following sections.

141 Field observations during the spring and early summer of 2008 revealed that the major portion
142 of the dune sites were bare, with the exception of Kelso and Little Sahara that contained sparse desert
143 grasses and reeds on the outer perimeter of the dune field and in some interdunal areas. Nonetheless,
144 this does not mean the other seven dune sites did not have vegetation in the past, since 2000. Table 2
145 shows that the spatial variation in emissivity for these two sites was small and less than 1%, and most
146 likely a result of the sampling sites being restricted to the central non-vegetated areas away from the
147 dune site perimeter.

148 The gypsum dunes at White Sands provide a good stability test for a NAALSED validation
149 target as the dunes migrate by up to 10 m per year in the northeasterly direction (McKee 1966)
150 resulting in an ever-changing landscape in which the dry dune crests, interdune areas and plant-life are
151 constantly changing and adapting over time. Furthermore, gypsum emissivity in band 11 (8.6 μm) is
152 particularly sensitive to soil moisture changes. Laboratory measurements show variations in gypsum
153 emissivity from 0.74 for a dry sample and up to 0.88 for a wetter sample (Mira et al. 2009). White
154 Sands had the largest, although still relatively small, temporal emissivity variation of 3.1% in band 11
155 (8.6 μm) of all dune sites using eleven ASTER scenes from 2003-2008 (Table 2). A similar result by
156 French et al. (2008) found no significant change in band 11 (8.6 μm) emissivity (<0.3% change per
157 year) from 2001-2003 at White Sands using nine ASTER scenes.

158 The presence of soil moisture would result in a significant increase in TIR emissivity at the
159 dune sites, caused by the water film on the sand particles decreasing its reflectivity (Mira et al. 2007;
160 Ogawa et al. 2006), particularly for ASTER bands 10-12 in the quartz Reststrahlen band. However,
161 given that the majority of dunes sites in this study are aeolian (high winds), at high altitude (low
162 humidity), and in semi-arid regions (high skin temperatures), the lifetime of soil moisture in the first
163 few micrometers of the surface skin layer as measured in the TIR is most likely small due to large
164 sensible heat fluxes and therefore high evaporation rates, in addition to rapid infiltration.

165 Consequently, we hypothesize that it would most likely take a very recent precipitation event to have
166 any noticeable effect on remote sensing observations of TIR emissivity over these types of areas.

167 Precipitation data from the Tropical Rainfall Measuring Mission (TRMM;
168 <http://trmm.gsfc.nasa.gov>) was analyzed for one week preceding each ASTER observation time for
169 each of the dune sites in order to observe possible soil moisture effects on emissivity. It should be
170 noted that a common phenomenon in desert areas is for rainfall to evaporate prior to hitting the Earth's
171 surface, and since TRMM is a cloud-top measure, there may be instances when rainfall was estimated,
172 but the surface remained dry. The results for Coral Pink Sands showed that TRMM data indicated
173 precipitation within two days of an ASTER observation for six out of a total of thirteen observations at
174 this site. The emissivity however, did not change by an appreciable amount (<2%), except for an
175 ASTER observation on 8 March 2002 at 18:21:52 UTC, which had an emissivity of approximately
176 15% higher than the dry emissivity value in bands 10-12. TRMM data indicated precipitation of up to
177 1.5 mm/hr at 00 UTC and 06 UTC the previous day, and an ASTER visible image over the area
178 showed a significant percentage of snow cover over the dunes due to a winter storm that had moved
179 through the area. As a result, all observations over the validation sites affected by precipitation were
180 deleted for comparisons with the lab results, where only dry samples were measured. These included

181 two out of a total of thirteen observations at Coral Pink Sands where snow cover increased the
182 emissivity in bands 10-12 by 15% and 5%, and two out of eleven at Killpecker dunes in Wyoming
183 when snow cover increased the retrieved emissivities by up to 15%.

184 Figure 2 shows box and whisker plots of ASTER emissivity in all five bands and surface
185 temperature at all nine sand dune sites using all observations during the winter (Jan-Mar) and summer
186 (Jul-Sep) from 2000-2008. The four observations affected by precipitation, as discussed above, were
187 excluded. The boxes have lines at the lower quartile, median (center line), and upper quartile values.
188 Whiskers extend from each end of the box to the to the minimum and maximum values, excluding the
189 outliers. Outliers are data with values beyond the ends of the whiskers and are displayed with a +
190 symbol. The boxplots give a good indication of the spread and skewness of data, and identifying
191 outliers, which provides a useful method for assessing the stability of the dunes over time in the
192 absence of precipitation effects.

193 From the boxplots, band 10 (8.3 μm) had the smallest degree of emissivity variation (<1%) at
194 all dunes sites, a surprising result since band 10 is the most susceptible to atmospheric effects. The
195 Algodones dunes and White Sands had the largest spread (~3%) in band 11 (8.6 μm), with Algodones
196 again showing a larger variation in band 14 (11.3 μm) which could be attributed to atmospheric
197 correction problems due to the summer monsoonal period in this region. Bands 12 (9.1 μm) and 13
198 (10.6 μm) had similar dispersions of roughly 1-2% at all dune sites.

199 The left panels in Figure 3 show the temporal emissivity variation at Kelso and Stovepipe
200 Wells dunes which both had the largest number of observations since 2000. The right panels show the
201 corresponding variation in Land Surface Temperature (LST) and NDVI. The temporal standard
202 deviations in emissivity at the two sites are small; 1.2% at Kelso, and 1.4 % at Stovepipe Wells for
203 band 11, although the LST's have much large variations between 300 and 330 K. The lack of

204 vegetation at both sites is evident in the low and unchanging NDVI values of between 0 and 1. In fact,
205 Table 2 shows that NDVI at all dune sites is less than 0.11, with variations not exceeding 0.05. The
206 correlations between emissivity and LST for both Kelso and Stovepipe in Figure 3 are small (0.16 and
207 0.08) which is expected since emissivity is an independent measurement to LST. The emissivity and
208 NDVI showed even smaller correlations (0.06 and 0.001) due to the lack of vegetation.

209

210 **3.2 Laboratory Measurements**

211

212 *Sampling Method*

213

214 Sand samples at each of the nine sand dune sites were collected during five separate field
215 campaigns in 2008, except for Moses Lake basalt samples which were provided courtesy of Dr. Joshua
216 Bandfield (Bandfield et al. 2002). Samples were collected at intervals of approximately 100 m over an
217 area roughly equivalent to 100 ASTER pixels (1 km×1 km). Sampling areas included the crests,
218 troughs, windward and leeward slopes of the dunes. The location of each sample was recorded by
219 GPS. Samples were collected by scooping the upper most few millimeters of the surface of the dunes
220 which most closely represents what the satellite instrument observes in the TIR.

221

222 *Reflectance and X-ray Diffraction Measurements*

223

224 The emissivity of the field samples was determined using a Nicolet 520 FT-IR spectrometer
225 equipped with a Labsphere integrating sphere (Baldrige et al. 2009). Each spectrum was then

226 convolved with the appropriate ASTER system response function. The uncertainty associated with the
227 Nicolet FT-IR emissivities is 0.002 (0.2 %) (Korb et al. 1999).

228 X-Ray Diffraction (XRD) was measured for all samples at Arizona State University using the
229 Rigaku D/Max-IIB. Samples were powdered and mounted on glass slides and scanned over the full 2 θ
230 range at a scan rate of 2 second per step at intervals of 0.020°. XRD peak lists were compared against
231 the full International Catalog of Diffraction Data (ICDD) powder database for bulk mineral analysis.
232 Each sample was also sorted and sieved. The mineralogy of each dune site and the associated sample
233 characteristics are shown in Table 1.

234

235 **4. DISCUSSION**

236

237 The sand dunes chosen for the validation study together include a wide range of materials,
238 including lithic fragments, pure quartz, gypsum, and feldspar and cover a wide range of emissivities in
239 the 8-12 μm range. Using the GPS sampling coordinates, emissivity data from NAALSED were
240 extracted for each sample site, using on average ten 100 m pixels per site. Figure 4 shows ASTER
241 false-color visible images of each dune site, and comparisons between the emissivity spectra from
242 NAALSED and the lab measurements. The visible images give an indication of the size, shape, color
243 and surrounding topography of the dunes, and sampling sites are indicated with blue dots surrounded
244 by rectangles. The lab spectra in Figure 4 give the mean and standard deviation (spatial) in emissivity
245 for all sand samples collected, while the NAALSED spectra give the mean emissivity and combined
246 spatial and temporal standard deviation for all observations acquired during the winter (Jan-Mar) and
247 summer (Jul-Sep) time periods. The results show that ASTER captures the spectral shape of all the
248 dune sands very well. The quartz doublet centered around band 11 (8.6 μm) is clearly visible for Coral

249 Pink and Algodones Dunes samples, and the characteristic gypsum minimum in band 11 (8.6 μm) is
250 evident from the White Sands samples.

251 The lab measurements from Kelso dunes showed the largest spatial variation in emissivity, with
252 standard deviations greater than 2.5% in bands 10 (8.3 μm), 11 (8.6 μm), and 12 (9.1 μm). This is a
253 result of four samples taken from dune crests containing traces of magnetite and amphibole, increasing
254 the emissivity by up to 3%. Differences between NAALSED and lab emissivities at White Sands for
255 band 11 (8.6 μm) were 2.75%, almost three times larger than in other bands which had differences of
256 less than 1%. This indicates a higher sensitivity to environmental changes for gypsum in band 11.

257 Table 3 gives a summary of the emissivity differences between NAALSED and the lab results
258 for each dune site and for all five TIR bands. The last column shows the absolute mean emissivity
259 difference, which is simply the mean bias of all five bands for each site. The results show that six out
260 of nine dune sites have excellent agreement with the lab results, in both spectral shape and magnitude,
261 with absolute differences of less than 1.5% (~1 K LST error). Two sites had differences of 1.7% (Little
262 Sahara) and 2.4% (Killpecker). TES was unable to capture the very deep quartz feature at Coral Pink
263 Sands, which had emissivities of less than 0.65 in bands 10-12, with a result that this site had the
264 largest differences with values of up to 7.5% (~5.6 K LST error) in bands 10-12, and less than 2.5% in
265 bands 13-14. Emissivity differences at all sites were primarily in amplitude, rather than spectral shape,
266 and five sites had systematic positive biases in all five ASTER bands.

267

268 **5. CONCLUSIONS**

269

270 The North American ASTER Land Surface Emissivity Database (NAALSED) version 2.0 has
271 been validated using a set of sand dune sites which encompass the range of expected surface

272 emissivities for bare surfaces in the TIR. The NAALSED database consists of a mean, seasonal,
273 gridded ASTER Land Surface Temperature and Emissivity (LSTE&E) product using all ASTER data
274 acquired from 2000 to 2008 during the winter (Jan-Mar) and summer (Jul-Sep).

275 Validation over arid and semi-arid regions was performed by collecting in-situ sand samples at
276 nine medium to large sand dune sites in the western/southwestern USA. Sand dune sites have been
277 found to be suitable targets for the validation of emissivity data due to their consistent and
278 homogeneous mineralogy and physical properties over long time periods. Temporal emissivity
279 variations for ASTER band 11 (8.6 μm) were generally less than 2% at all dune sites, with White
280 Sands having the largest variation of 3.1%. Spatial variations were smaller, and less than 1.5% at all
281 sites.

282 NAALSED and lab emissivity spectra showed very good agreement in amplitude and spectral
283 shape at six out of nine dune sites with an average combined difference using all five ASTER TIR
284 bands of less than 1.5% (~ 1 K), which include a wide range of emissivities from 0.6 - 0.96 in the 8-12
285 μm range. These differences fall within the initial ASTER emissivity accuracy of 1.5% determined
286 using numerical simulations (Gillespie et al. 1998). Two sites had differences ranging from 1.5 - 2.5%,
287 while Coral Pink Sands had the largest absolute mean difference of 5.1%. The combined mean
288 emissivity difference between NAALSED and the laboratory results for all nine validation sites and all
289 five ASTER TIR bands was 1.6 %. This emissivity difference is equivalent to approximately a 1 K
290 error in the land surface temperature for a material at 300 K in the TIR.

291 These results indicate that the TES algorithm works well over arid and semi-arid regions and
292 opens up the potential for using NAALSED to intercompare and validate LST&E products from other
293 sensors with much coarser spatial resolution such as AIRS (45 km), MODIS (5 km) and MSG/SEVIRI
294 (3 km).

295

296 **Acknowledgements.** The research described in this paper was carried out at the Jet Propulsion
297 Laboratory, California Institute of Technology, under the contract with the National Aeronautics and
298 Space Administration. We kindly thank Dr. Tom Schmutge from New Mexico State University for
299 assisting us with field work at White Sands, and also Dr. Joshua Bandfield for providing the basalt
300 samples from Moses Lake, WA. ASTER data was provided by
301 NASA/GSFC/METI/ERSDAC/JAROS, and U.S./Japan ASTER Science Team.

302

303 **References**

304

305 Baldridge, A.M., Hook, S.J., Grove, C.I., & Rivera, G. (2009). The ASTER Spectral Library Version
306 2.0. *Remote Sensing of Environment*, 114, (4), 711-715

307 Bandfield, J.L., Edgett, K.S., & Christensen, P.R. (2002). Spectroscopic study of the Moses Lake dune
308 field, Washington: Determination of compositional distributions & source lithologies. *Journal of*
309 *Geophysical Research-Planets*, 107, (E11), 5092

310 Bannari, A., Omari, K., Teillet, R.A., & Fedosejevs, G. (2005). Potential of getis statistics to
311 characterize the radiometric uniformity and stability of test sites used for the calibration of earth
312 observation sensors. *Ieee Transactions on Geoscience and Remote Sensing*, 43, (12), 2918-2926

313 Bonan, G.B., Oleson, K.W., Vertenstein, M., Levis, S., Zeng, X.B., Dai, Y.J., Dickinson, R.E., &
314 Yang, Z.L. (2002). The land surface climatology of the community land model coupled to the NCAR
315 community climate model. *Journal of Climate*, 15, (22), 3123-3149

- 316 Coll, C., Sánchez, J.M., Caselles, V., Valor, E., Niclòs, R., & Galve, J.M. (2005). Validation of
317 ASTER derived surface temperatures and emissivities with ground measurements. *Geophysical*
318 *Research Abstracts*, 7, (-), 06440
- 319 Cosnefroy, H.N., Leroy, M., & Briottet, X. (1996). Selection and characterization of Saharan and
320 Arabian desert sites for the calibration of optical satellite sensors. *Remote Sensing of Environment*, 58,
321 (1), 101-114
- 322 de Vries, C., Danaher, T., Denham, R., Scarth, P., & Phinn, S. (2007). An operational radiometric
323 calibration procedure for the Landsat sensors based on pseudo-invariant target sites. *Remote Sensing of*
324 *Environment*, 107, (3), 414-429
- 325 French, A.N., Schmugge, T.J., Ritchie, J.C., Hsu, A., Jacob, F., & Ogawa, K. (2008). Detecting land
326 cover change at the Jornada Experimental Range, New Mexico with ASTER emissivities. *Remote*
327 *Sensing of Environment*, 112, (4), 1730-1748
- 328 Gillespie, A., Rokugawa, S., Matsunaga, T., Cothorn, J.S., Hook, S., & Kahle, A.B. (1998). A
329 temperature and emissivity separation algorithm for Advanced Spaceborne Thermal Emission and
330 Reflection Radiometer (ASTER) images. *Ieee Transactions on Geoscience and Remote Sensing*, 36,
331 (4), 1113-1126
- 332 Hook, S.J., Vaughan, R.G., Tonooka, H., & Schladow, S.G. (2007). Absolute radiometric in-flight
333 validation of mid infrared and thermal infrared data from ASTER and MODIS on the terra spacecraft
334 using the Lake Tahoe, CA/NV, USA, automated validation site. *Ieee Transactions on Geoscience and*
335 *Remote Sensing*, 45, (6), 1798-1807
- 336 Hulley, G.C., & Hook, S.J. (2008). A new methodology for cloud detection and classification with
337 ASTER data. *Geophysical Research Letters*, 35, (16), L16812, doi: 16810.11029/12008gl034644

- 338 Hulley, G.C., & Hook, S.J. (2009a). Intercomparison of Versions 4, 4.1 and 5 of the MODIS Land
339 Surface Temperature and Emissivity Products and Validation with Laboratory Measurements of Sand
340 Samples from the Namib Desert, Namibia. *Remote Sensing of Environment*, doi:
341 10.1016/j.rse.2009.1002.1018
- 342 Hulley, G.C., & Hook, S.J. (2009b). The North American ASTER Land Surface Emissivity Database
343 (NAALSED) Version 2.0. *Remote Sensing of Environment*, In Press
- 344 Hulley, G.C., Hook, S.J., & Baldrige, A.M. (2008). ASTER land surface emissivity database of
345 California and Nevada. *Geophysical Research Letters*, 35, (13), L13401, doi:
346 10.1029/2008gl034507
- 347 Jin, M.L., & Liang, S.L. (2006). An improved land surface emissivity parameter for land surface
348 models using global remote sensing observations. *Journal of Climate*, 19, (12), 2867-2881
- 349 Korb, A.R., Salisbury, J.W., & D'Aria, D.M. (1999). Thermal-infrared remote sensing and Kirchhoff's
350 law 2. Field measurements. *Journal of Geophysical Research-Solid Earth*, 104, (B7), 15339-15350
- 351 Kornfield, J., & Susskind, J. (1977). Effect of Surface Emissivity on Temperature Retrievals. *Monthly
352 Weather Review*, 105, (12), 1605-1608
- 353 McKee, E.D. (1966). Structures of Dunes at White Sands National Monument, New Mexico (and a
354 Comparison with Structures of Dunes from other Selected Areas). *Sedimentology*, 7, 1-69
- 355 Mira, M., Schmugge, T., Valor, E., Caselles, V., & Coll, C. (2009). Comparison of Thermal Infrared
356 Emissivities Retrieved With the Two-Lid Box and the TES Methods With Laboratory Spectra. *Ieee
357 Transactions on Geoscience and Remote Sensing*, 47, (4), 1012-1021
- 358 Mira, M., Valor, E., Boluda, R., Caselles, V., & Coll, C. (2007). Influence of soil water content on the
359 thermal infrared emissivity of bare soils: Implication for land surface temperature determination.
360 *Journal of Geophysical Research-Earth Surface*, 112, (F4), F04003

- 361 Mushkin, A., & Gillespie, A.R. (2005). Estimating sub-pixel surface roughness using remotely sensed
362 stereoscopic data. *Remote Sensing of Environment*, 99, (1-2), 75-83
- 363 Ogawa, K., Schmugge, T., & Rokugawa, S. (2006). Observations of the dependence of the thermal
364 infrared emissivity on soil moisture. *Geophysical Research Abstracts*, 8, (-), 04996
- 365 Schmugge, T., & Ogawa, K. (2006). Validation of Emissivity Estimates from ASTER and MODIS
366 Data, *Proceedings of 2006 International Geoscience and Remote Sensing Symposium* (pp. 260-262)
- 367 Schmugge, T., Ogawa, K., Jacob, F., French, A., Hsu, A., & Ritchie, J.C. (2003). Validation of
368 Emissivity Estimates from Aster Data *Proceedings of 2003 International Geoscience and Remote*
369 *Sensing Symposium* (pp. 1873-1875)
- 370 Seemann, S.W., Borbas, E.E., Knuteson, R.O., Stephenson, G.R., & Huang, H.L. (2008). Development
371 of a global infrared land surface emissivity database for application to clear sky sounding retrievals
372 from multispectral satellite radiance measurements. *Journal of Applied Meteorology and Climatology*,
373 47, (1), 108-123
- 374 Susskind, J., Barnet, C.D., & Blaisdell, J.M. (2003). Retrieval of atmospheric and surface parameters
375 from AIRS/AMSU/HSB data in the presence of clouds. *Ieee Transactions on Geoscience and Remote*
376 *Sensing*, 41, (2), 390-409
- 377 Teillet, P.M., Fedosejevs, G., Gautier, R.P., & Schowengerdt, R.A. (1998). Uniformity characterization
378 of land test sites used for radiometric calibration of earth observation sensors, *Proc. 20th Can. Symp.*
379 *Remote Sensing* (pp. 1-4). Calgary, AB, Canada
- 380 Tonooka, H., & Palluconi, F.D. (2005). Validation of ASTER/TIR standard atmospheric correction
381 using water surfaces. *Ieee Transactions on Geoscience and Remote Sensing*, 43, (12), 2769-2777
- 382 Wan, Z.M. (2008). New refinements and validation of the MODIS Land-Surface
383 Temperature/Emissivity products. *Remote Sensing of Environment*, 112, (1), 59-74

384 Zhou, L., Dickinson, R.E., Tian, Y., Jin, M., Ogawa, K., Yu, H., & Schmugge, T. (2003). A sensitivity
385 study of climate and energy balance simulations with use of satellite-derived emissivity data over
386 Northern Africa and the Arabian Peninsula. *Journal of Geophysical Research-Atmospheres*, 108,
387 (D24), 4795
388
389

Table 1. Summary of the major characteristics of each dune site including locality, elevation, surface area, dune height, grain size, sand source and bulk mineralogy.

Dune site	Locality	Surface Area (km²)	Elevation/ Max Dune Height (m)	Grain Size	Sand Source	Mineralogy (XRD)
Algodones 32.95 N, 115.07 W	Southeast CA, Eastern margin of the Salton Trough	720	94/80	Medium to Coarse Sand	Beach sand from Lake Cahuilla	Major: Quartz
Coral Pink 37.04 N, 112.72 W	Sand Valley, just north of UT-AZ border, west Kanab	13.6	1780/10	Medium Sand	Navajo, Page and Estrada Jurassic sandstones of the Vermillion Cliffs	Major: Quartz
Great Sands 37.77 N, 105.54 W	San Luis Valley, CO, adjacent to Sangre de Cristo, NE of Alamosa	104	2560/230	Medium to Coarse Sand	Quartz and volcanic fragments derived from Santa Fe and Alamosa formations, recent fluvial (Rio Grande) deposits	Major: Quartz Minor: Potassium Feldspar
Kelso 34.91 N 115.73 W	Mojave Desert, CA, southeast of Baker	115	800/195	Medium Sand	Derived from sedimentary, metamorphic, igneous terrains from Mojave River alluvial apron	Major: Quartz Minor: Potassium Feldspar Trace: Magnetite
Killpecker 41.98 N 109.10 W	Southwest WY, from Eden across Rock Springs into Red Desert	550	2000/45	Medium Sand	Sandstone and siltstone of the Laney member of the Green River Formation	Major: Quartz Minor: Plagioclase Feldspar, Epidote Trace: Magnetite
Little Sahara/ Lynndyl 39.7 N 112.39 W	West-central UT, Sevier River drainage basin, west of Lynndyl	575	1560/200	Fine Sand	Deltaic and shoreline sediments from the Provo shoreline of Lake Bonneville	Major: Quartz Minor: Plagioclase Feldspar, Pyroxene, Carbonate, Magnetite
Stovepipe Wells 36.62 N, 117.11 W	Central Death Valley, CA, near Stovepipe Wells	7.7	-12/40	Medium Sand	Mixed lithic fragments and quartz from Emigrant Pass to the west and Furnace Wash to the east	Major: Quartz Minor: Plagioclase Feldspar, Potassium Feldspar
Moses Lake 47.05 N, 119.31 W	Quincy Basin in central WA	40	345/18	Fine Sand	Basaltic sand from the east bank of the Columbia River	Major: Quartz, Albite
White Sands 32.89 N, 106.33 W	South-central NM, Tularosa Valley	704	1216/10	Fine Sand	Paleo-lake Otero, present playa Lake Lucero to the southwest	Major: Gypsum

Table 2. NAALSED temporal and spatial variations for each dune site, showing values for the total number of observations, mean NDVI, temporal NDVI variation (δNDVI), temporal emissivity variation ($\delta\varepsilon_t$) and spatial emissivity variation ($\delta\varepsilon_s$) for band 11 (8.6 μm) using all ASTER observations from 2000-2008.

Dune site	Obs	NDVI	δNDVI	$\delta\varepsilon_t$ (%)	$\delta\varepsilon_s$ (%)
Algodones	21	0.09	0.014	2.2	1.2
Stovepipe Wells	20	0.05	0.014	1.0	0.3
White Sands	11	0.10	0.050	3.1	1.2
Kelso	24	0.09	0.009	1.8	0.9
Great Sands	6	0.11	0.006	1.7	0.9
Moses Lake	4	0.11	0.023	1.1	1.5
Coral Pink	13	0.11	0.028	1.4	0.2
Little Sahara	11	0.09	0.025	2.0	0.3
Killpecker	6	0.09	0.015	1.2	0.2

Table 3. Mean emissivity differences between NAALSED and laboratory emissivities (%) for ASTER bands 10-14 using all available ASTER data from 2000-2008. The last column shows the absolute mean emissivity difference (mean bias) for all bands.

Dune site	NAALSED minus Lab Emissivity (%)					Mean
	Band 10	Band 11	Band 12	Band 13	Band 14	
Algodones	-0.7	-0.6	-0.1	0.04	-1.4	0.6
Stovepipe Wells	0.3	-0.5	-0.7	0.4	-0.4	0.5
White Sands	-0.6	1.7	-0.4	-0.7	-1.1	0.9
Kelso Dunes	1.6	1.1	1.4	1.9	0.8	1.4
Great Sands	1.4	1.0	1.4	1.6	0.7	1.2
Moses Lake	-0.6	-0.4	0.5	0.7	-1.0	0.7
Coral Pink	7.5	6.5	7.4	2.5	1.7	5.1
Little Sahara	3.2	2.0	2.1	1.0	0.2	1.7
Killpecker	3.2	3.0	3.4	1.6	0.8	2.4

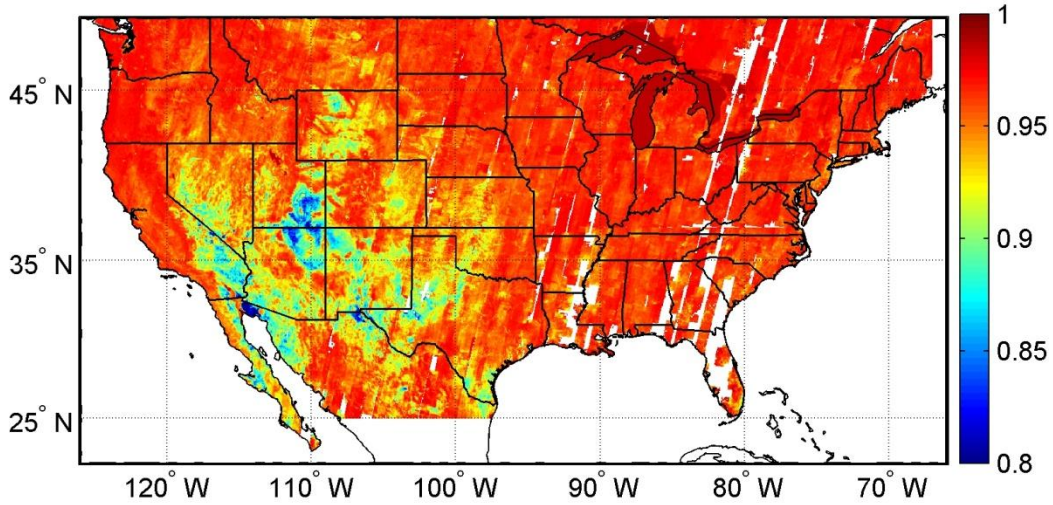


Figure 1. NAALSED mean Summer (Jul-Sep) emissivity for band 12 (9.1 μm) using 70,075 ASTER scenes acquired from 2000-2008. White areas over land had no clear sky coverage and plan to be filled during the 2009 Summer acquisition period.

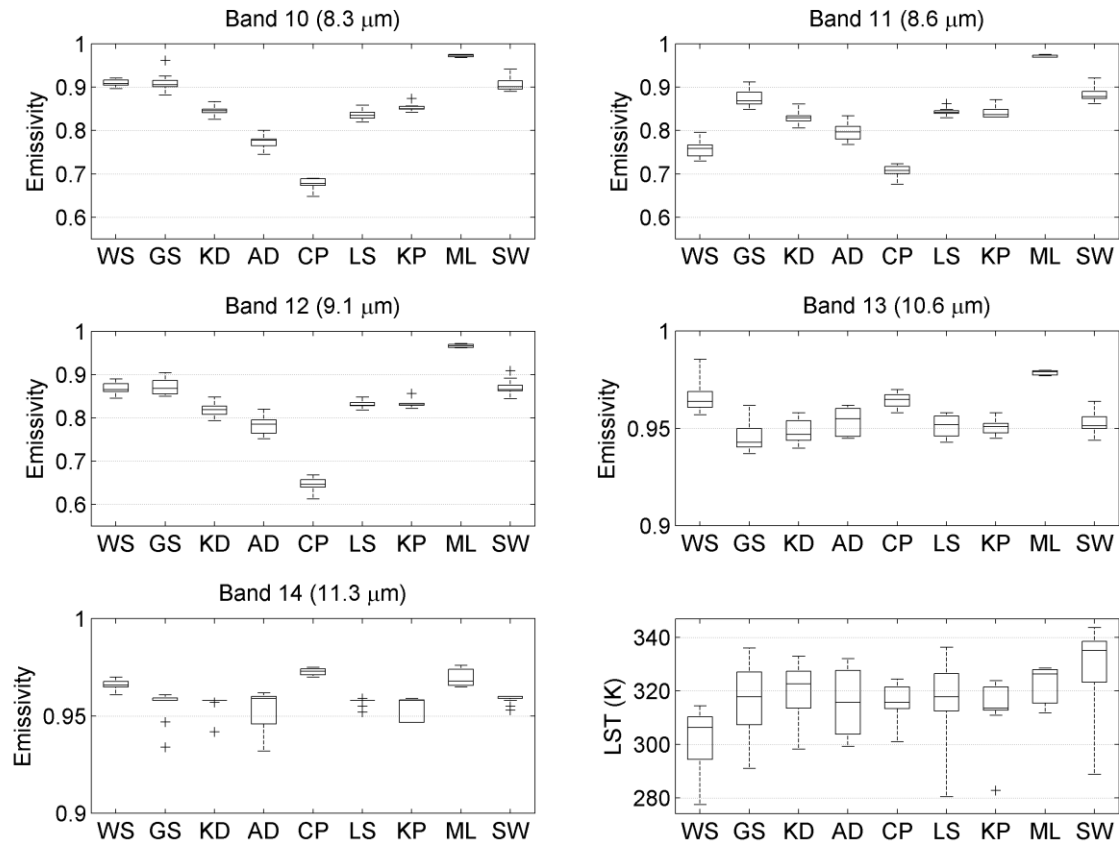


Figure 2. Box-and-whisker plots showing ASTER emissivity and Land Surface Temperature (LST) variation for dune sites: White Sands (WS), Great Sands (GS), Kelso Dunes (KD), Algodones Dunes (AD), Coral Pink (CP), Little Sahara (LS), Killpecker (KP), Moses Lake (ML), and Stovepipe Wells (SW). The boxes have lines at the lower quartile, median (center line), and upper quartile values, with whiskers extending from each end of the box to the adjacent values in the data. Outliers are displayed with a + symbol.

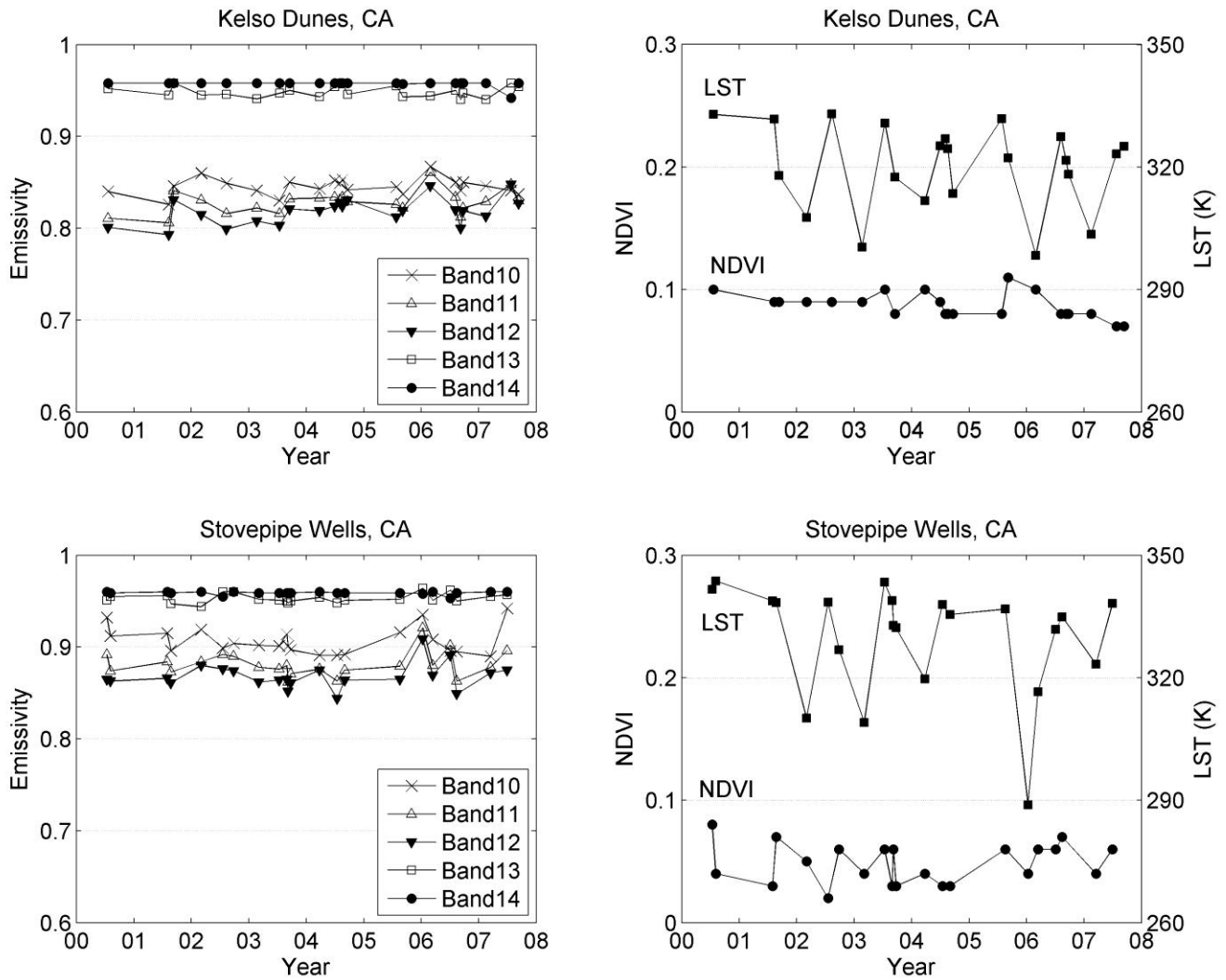


Figure 3. ASTER temporal emissivity changes for all five bands (left panels), and corresponding NDVI and Land Surface Temperature (LST) variation (right panels), for Kelso Dunes (top panels) and Stovepipe Wells Dunes (bottom panels).

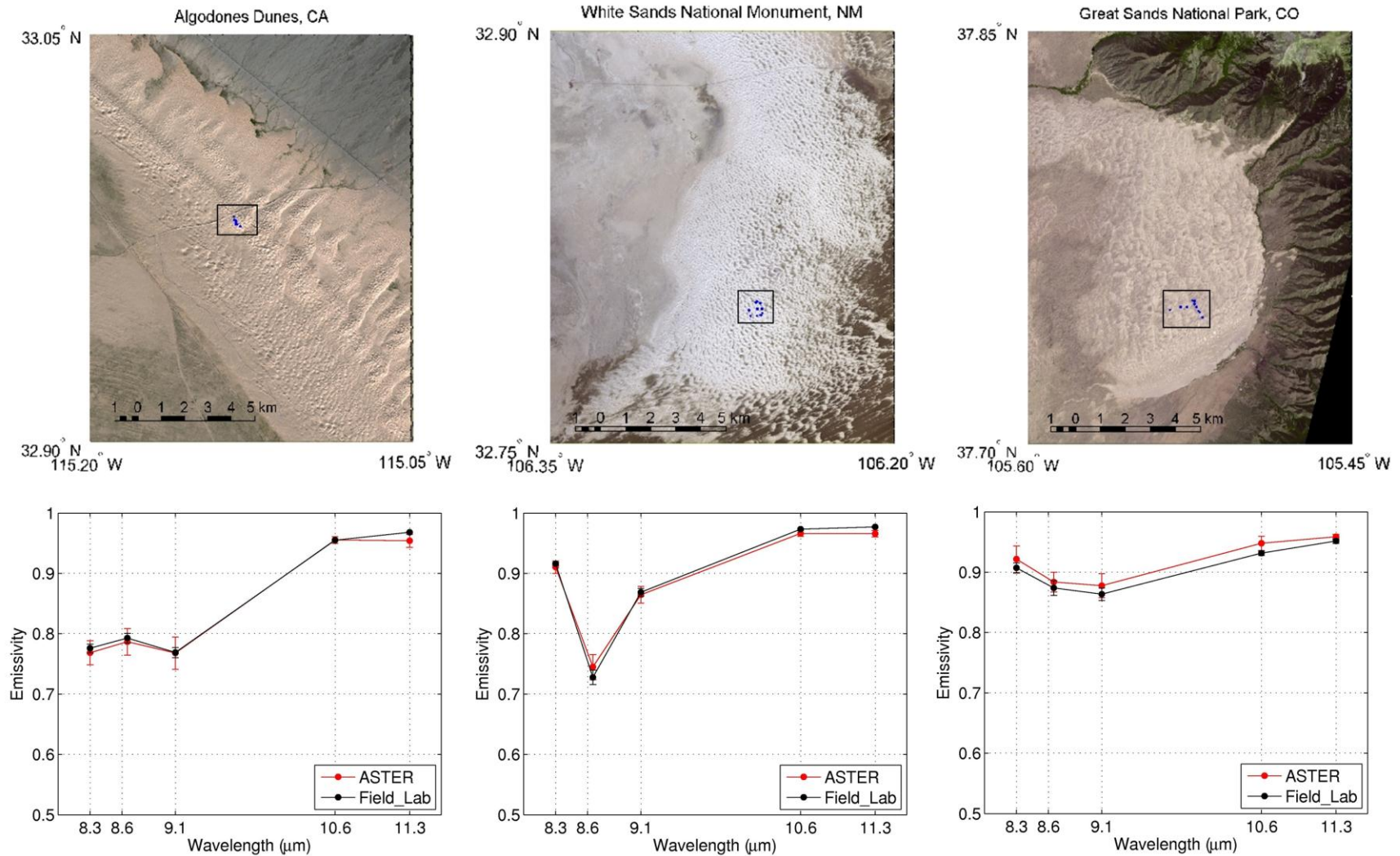


Figure 4. ASTER false-color visible images (top) and emissivity spectra comparisons between ASTER and lab results for Algodones Dunes, California; White Sands, New Mexico; and Great Sands, Colorado. Squares with blue dots indicate the sampling areas. ASTER error bars show temporal and spatial variation, whereas lab spectra show spatial variation.

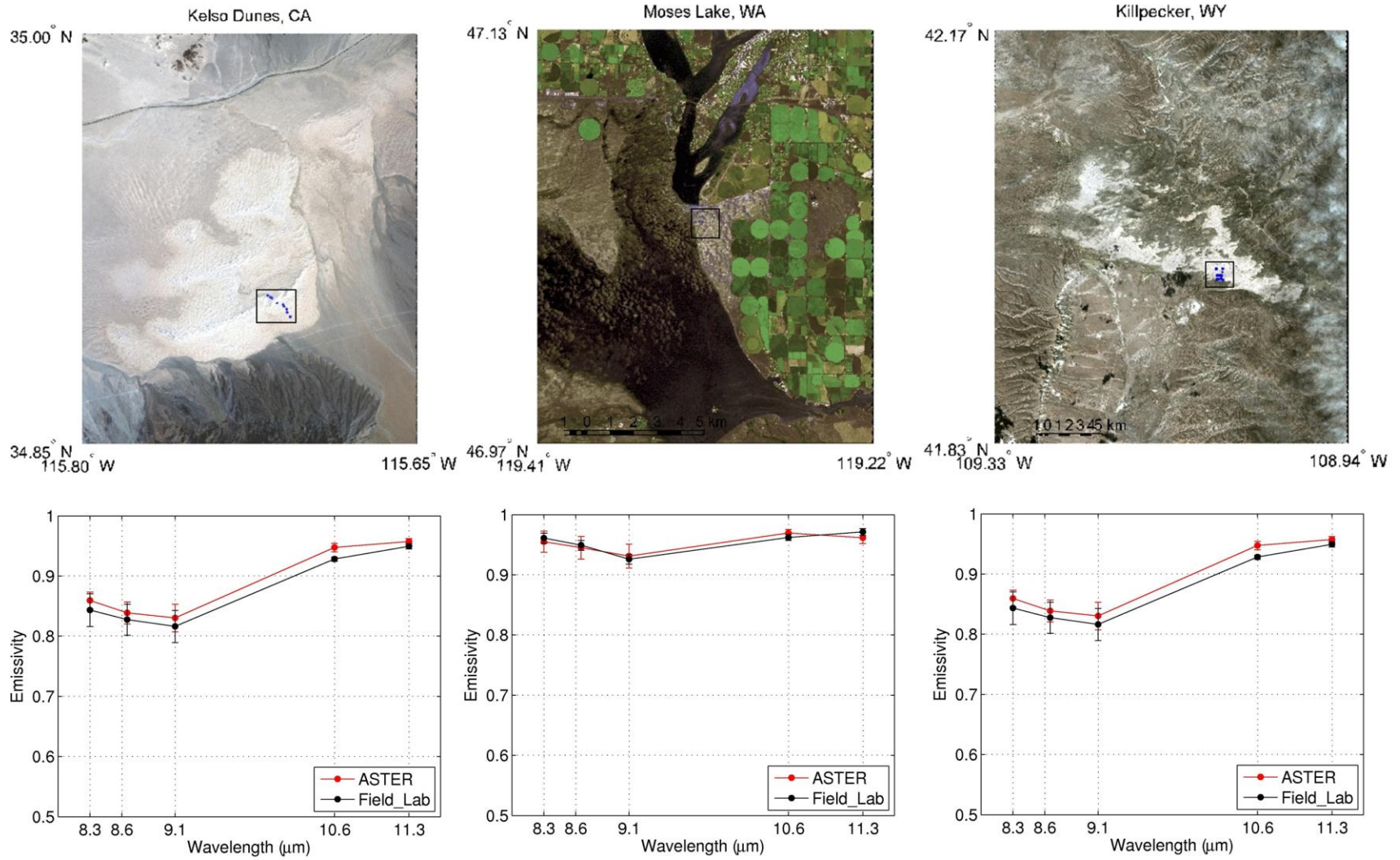


Figure 4 (continued). Validation results for Kelso Dunes, California; Moses Lake, Washington and Killpecker, Wyoming.

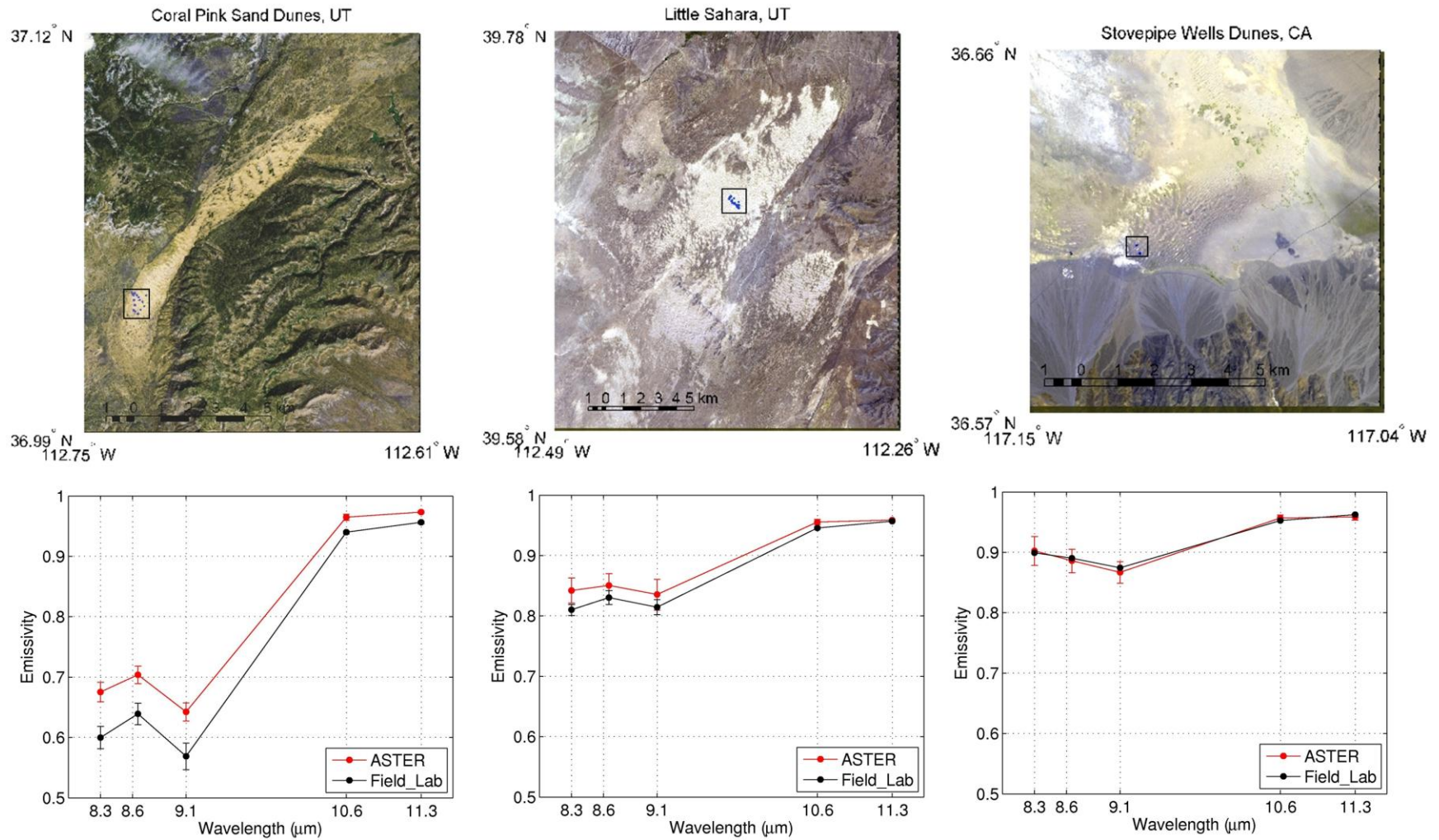


Figure 4 (continued). Validation results for Coral Pink Sands, Utah; Little Sahara, Utah and Stovepipe Wells, California.